Progress In Electromagnetics Research, PIER 24, 185–199, 1999

FDTD CHARACTERIZATION OF MEANDER LINE ANTENNAS FOR RF AND WIRELESS COMMUNICATIONS

C.-W. P. Huang, A. Z. Elsherbeni, J. J. Chen, and C. E. Smith

Electrical Engineering Department
The University of Mississippi
University, MS 38677, USA

1. INTRODUCTION

With the advancements of modern integrated circuit technologies, personal communication systems (PCS) are the fast growing sections of the present telecommunication industry. Modern designs of wireless personal communication systems are featured in light weigh, small size, high frequency operation, and high transmission efficiency. Mobile antenna design is one of the major tasks in PCS designs. In addition to the general features needed for PCS antennas for mobile personal communications, there is also a requirement that the antenna be easily integrated with the interior circuitry of the system. One of the most widely used wireless communications systems is the global system for mobile (GSM) communications, that operates at 890–915 MHz for uplink and 935–960 MHz for downlink. The new generation of personal communication systems, such as digital communication systems (DCS) 1800, operates at 1.710–1.785 GHz for uplink and 1.805–1.880 GHz for downlink. Therefore, antennas for current personal communication systems are required to operate at the frequency range form 0.9 GHz to 2.0 GHz . If the future use of higher frequency PCS and the

possibility of applying PCS for military purposes are considered, then antenna designs for wireless personal communication systems should be expanded in scope to cover the frequency range from the current 0.9–2.0 GHz to 0.9–3.0 GHz range. In this paper, studies for the characteristics of a printed meander line antenna [1–5], using the finite difference time domain (FDTD) techniques [6] with Berenger's perfectly matched layers (PML) absorbing boundaries [7] are presented. The presented designs of the antenna shown in Fig. 1(b), feature small dimensions $(77 \times 11 \times 3.17\,\mathrm{mm}^3)$, approximately $50\,\Omega$ input impedance, dual frequency operating in the 0.9–3.0 GHz band, and on a comparably small ground plane $(59 \times 25.4\,\mathrm{mm}^2)$. One of the validations of the numerical code used in this investigation is made by comparing the numerical results of the return loss of a rectangular printed patch antenna with the computed and measured data reported in [8, 9]. The analysis and empirical design equations for the input impedance, resonance and operating frequencies of meander line antennas with dual sleeves are provided.

2. ANALYSIS

The antenna considered in this investigation, as shown in Figure 1, is a meander line trace printed on a dielectric slab with printed sleeves (passive radiators) sitting on a perfectly conducting ground plane. The parameters $e1$ and $e2$ represent the lengths of the vertical and horizontal printed traces, respectively. In this study, $e1$ and $e2$ are chosen to be $3\,\mathrm{mm}$, and the width of the printed trace is $1\,\mathrm{mm}$. The parameter L_{ax} is the vertical length of the meander line. The distance between the edge of the dielectric slab and the edge of the ending segment of the meander line is set equal to $e1$. The reason for modeling the meander line antenna on a small ground plane $(59 \times 25.4\,\mathrm{mm}^2)$ is to simulate its performance when this antenna is placed on top of a PCS handset. The main objective of this research is to design a meander line antenna with $50\,\Omega$ input impedance at dual operating frequencies within 0.9 to $2.5\,\mathrm{GHz}$. Other important parameters are to minimize the size of the dielectric slab and the ground plane. The frequency range under study is extended form 0.9–3.0 GHz to 0.5–4.5 GHz for clearer observations of the resonance behavior of the antenna.

The finite difference time domain (FDTD) technique is applied to model the antenna inside a 3 dimensional air chamber terminated with 8 layers of the artificial boundaries based on Berenger's algorithm

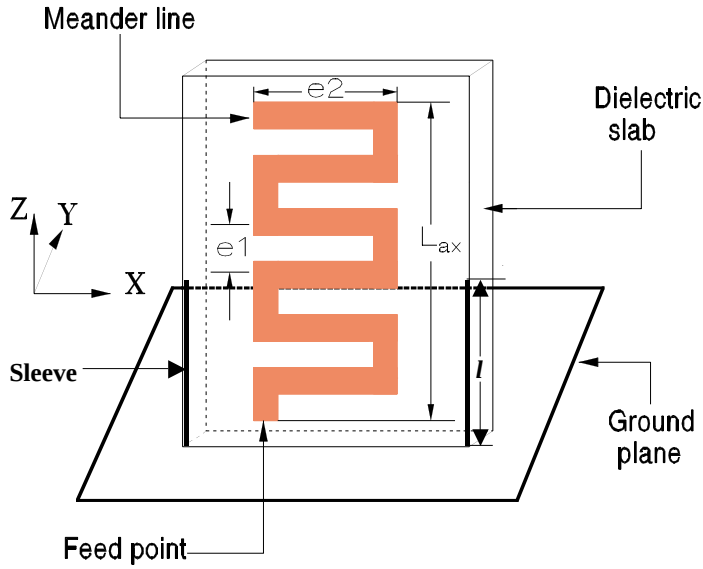

Figure 1. A meander line antenna on a small ground plane $(59 \times 25.4\,\mathrm{mm}^2)$.

PML [7]. The PML is adopted to reduce the numerical reflection from the truncated computational boundaries, which resembles the anechoic chamber for antenna measurements. An array of voltage sources with a Gaussian waveform is placed between the ground plane and the edge of the first vertical segment of the trace line for excitations.

To begin the meander line antenna design, the width (W_s) and thickness (t_s) of the dielectric slab are set to $3.17\,\mathrm{mm}$ and $11\,\mathrm{mm}$, respectively. The changes in impedance and resonant frequency are observed by increasing the number of segments of the meaner line trace gradually until the design goal is achieved. In [2–5], meander line antennae have $50\,\Omega$ input impedance when they are measured on a large ground plane or in dipole configuration. When the meander line is printed on a small substrate sitting on a small ground plane as shown in Figure 1, the input impedance reduces dramatically. In [2], dual sleeves have been successfully used to tune the wire meander line antenna to $50\,\Omega$ and widen the bandwidth. Therefore, dual sleeves are printed on both edges of the dielectric substrate with spacing equal to $e1$ (or $e2$). The length of the sleeves is adjusted for optimal matching. When the length of the sleeve is around half of L_{ax}, the input

impedance of the antenna is in the $50\,\Omega$ range, which agrees with the conclusions in [2]. Therefore, the study of unilaterally printed meander line antenna is begun with varying the L_{ax} and with the sleeve length l equal to $1/2L_{ax}$. The effects of dielectric constant, the widths and thickness of the slab are also studied. In this simulation, the values of the dielectric constant are varied between 2.2 and 10.2, while the thicknesses of dielectric slab are 0.794,1.588, 3.175, 4.763, and 6.35 mm to conform with commonly used materials for radio frequency (RF) and microwave circuit boards. The width of the dielectric slab is varied from 11 to 41 mm which is an appropriate width to be incorporated with a PCS handset. From these numerical experiments, empirical equations are derived to facilitate the design procedure.

3. NUMERICAL RESULTS

The computation of the return loss of a rectangular patch antenna presented in [8] as shown in Figure 2 is reported here as a validation for the developed code. The FDTD cell discretization and the dimensions of this patch antenna can be found in [8]. In Figure 2, good agreement between the computed numerical results and the published computed and measured data are observed. The necessary number of layers of air buffer between the patch antenna and the PML is also illustrated in this example. Reference [9] presents results obtained by placing 10 cells of PML on top of 5 cells of air above the patch and 3 cells of air away from the edge of the patch. In this paper, the number of PML layers used in all numerical cases is 8. In Figure 2, negligible difference is observed due to the placement of the PML 2 cells and 5 cells away from the top surface of the patch. Therefore, the PML layers can be placed very close to the antenna under study as concluded in [7, 9], which allows more computational resources for the problem space.

The input impedance of the initial design ($t_s = 3.17$ mm and $W_s = 11$ mm) of the meander line antenna with dual sleeves for various numbers of segments are plotted in Figure 3. As shown in the Figure, the increase of L_{ax} decreases all the resonant frequencies. The operating frequencies are the frequencies where the reflection coefficients are less than -20 dB as shown in Fig. 4. Due to the existence of the dual sleeves, the first resonance is around $10\,\Omega$ for these shown antennas (Fig. 5(b)). However, except for the antenna with $L_{ax} = 19$ mm, the 1st and 2nd operating frequencies of these antennas are found at the vicinities of the 3rd and 5th resonance frequen-

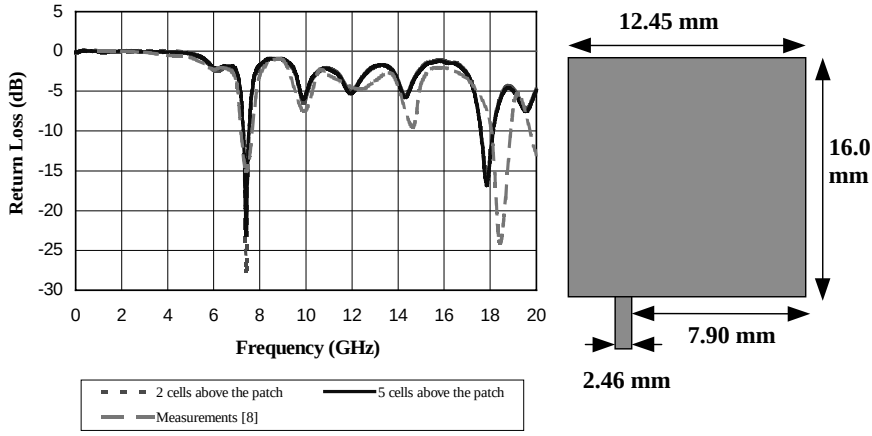

Figure 2. Magnitude of reflection coefficient of a rectangular patch antenna.

cies, respectively (Figs. 5(a) and 5(c)), whose corresponding resonance impedance is varied between 40 and $50\,\Omega$ and between 35 and $50\,\Omega$ (Fig. 5(b)). The first operating frequency (4.14 GHz) of the antennas with $L_{ax} = 19\,\text{mm}$ is between the 1st (2.5 GHz) and 3rd resonance (7.5 GHz), which is above the frequency range of the current PCS applications. Additionally, optimal cases can be found when using 42 segments (64 mm for L_{ax}) and 48 segments (73 mm for L_{ax}), where the 3rd and 5th resonance impedance is $42\,\Omega$ and $40\,\Omega$, $40.5\,\Omega$ and $47\,\Omega$, respectively. The 3rd and 5th resonant frequencies for these two designs are in the frequency range of 0.9 to 3.0 GHz, which indicate that for L_{ax} between 64 and 73 mm, dual frequencies operation is achievable within the current or future PCS applications. Furthermore, these antennas are adequately matched to the traditional $50\,\Omega$ impedance of the front-end circuitry. This $50\,\Omega$ input impedance feature should simplify the PCS system designs by removing the impedance matching network between the feed and the antenna. From Figure 5(d), the bandwidths of these antennas with L_{ax} between 64 and 73 mm are around 12% and 4.5% for the first and second operating frequencies, respectively. The empirical equations for the 1st and 2nd operating frequencies and 3rd and 5th resonance impedance for various values of L_{ax} are derived from regression curve-fit of the data plotted in Figure 5. The empirical equations for the operating frequencies are

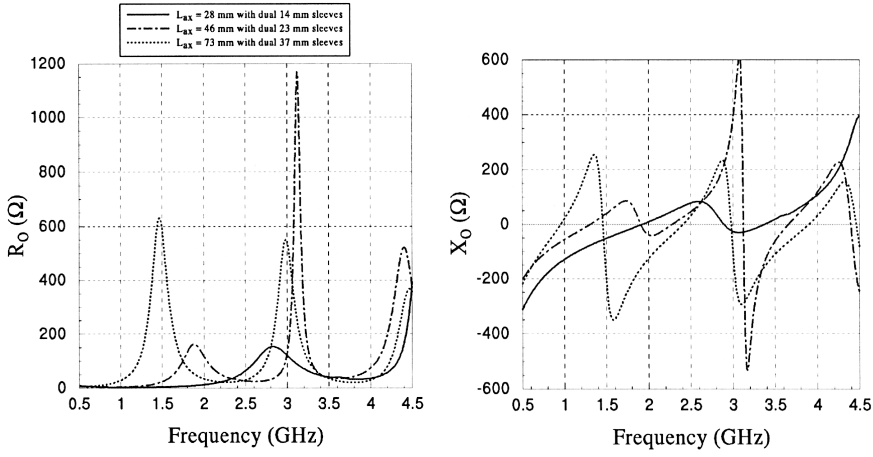

(a) (b)

Figure 3. (a) Real parts and (b) imaginary parts of the input impedance for meander line antennas with dual sleeves.

$$f_{op1} = 10.03 - 2.0143 \ln(L_{ax}) \tag{1a}$$

$$f_{op2} = 18.152 - 3.722511 \ln(L_{ax}) \tag{1b}$$

while the equations for the 3rd and 5th resonance impedance are given by

$$\begin{aligned} R_{o3} = {} & 9.8226 \times 10^{-8}(L_{ax})^6 - 2.5210 \times 10^{-5}(L_{ax})^5 + \\ & 0.0025026(L_{ax})^4 - 0.11898(L_{ax})^3 + \\ & 2.6549(L_{ax})^2 - 20.48(L_{ax}) \end{aligned} \tag{2a}$$

$$R_{o5} = 0.0096(L_{ax})^2 - 0.7454(L_{ax}) + 49.261 \tag{2b}$$

These empirical equations are for meander line antennas with dual sleeves ($l_1 = 1/2L_{ax}$) using 1 mm trace, $e1 = e2 = 3$ mm, $t_s = 3.17$ mm and $W_s = 11$ mm , substrate relative permittivity of 2.2, and a $59 \times 25.4\,\text{mm}^2$ ground plane. It is worth noting that the first operating frequency for L_{ax} within 46 and 64 mm featured a bandwidth of 12 percent that may support the upcoming 3rd generation cellular systems, operating around 2 GHz as shown in Fig. 5.

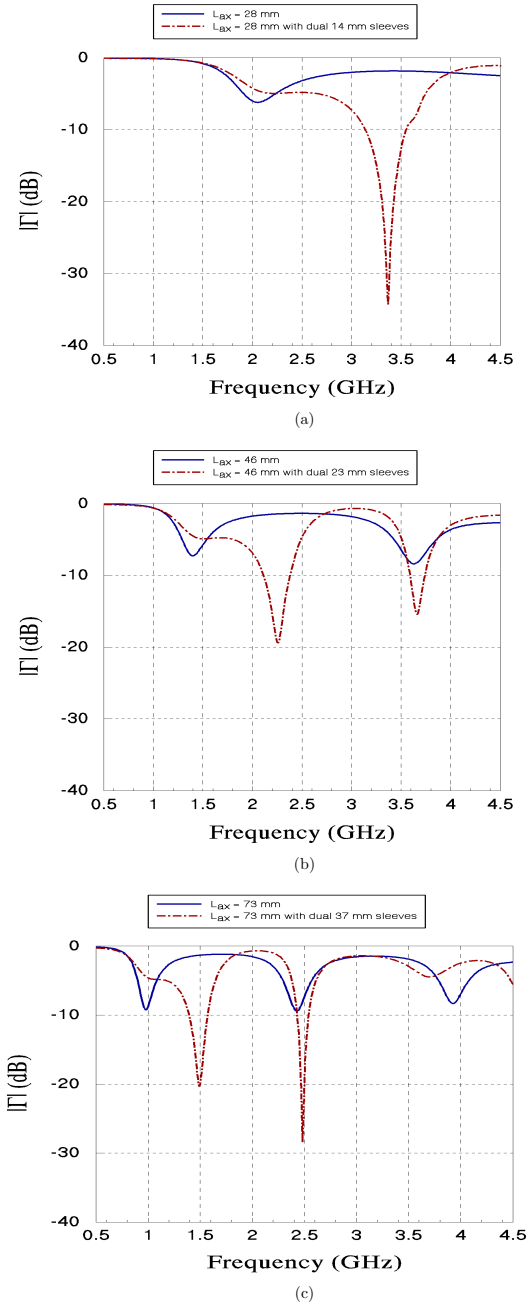

Figure 4. Magnitude of reflection coefficient of (a) 28 mm (b) 46 mm (c) 73 mm meander line antennas.

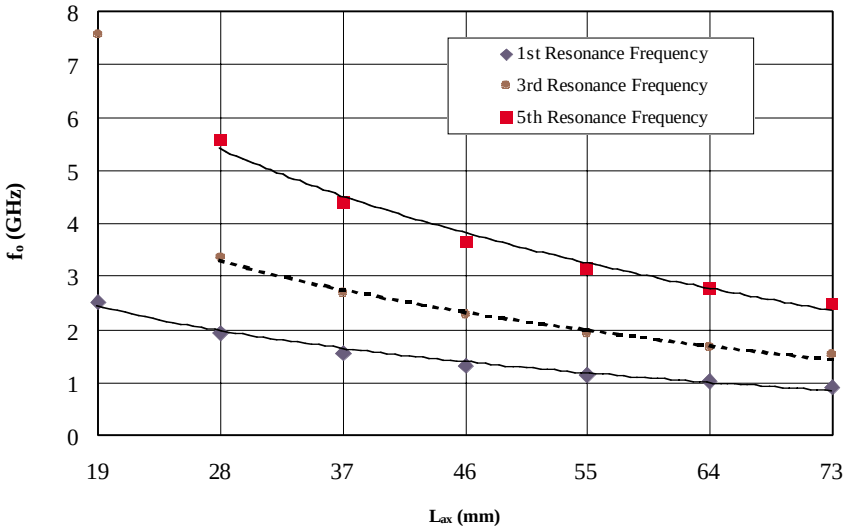

(a)

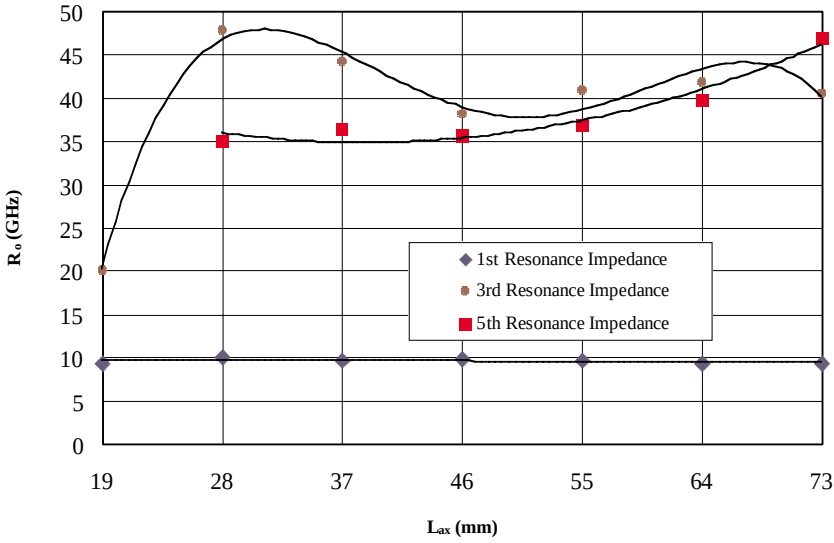

(b)

Figure 5. (a) Resonance frequencies (b) resonance impedance (c) operating frequencies (d) bandwidth of meander line antennas versus L_{ax} .

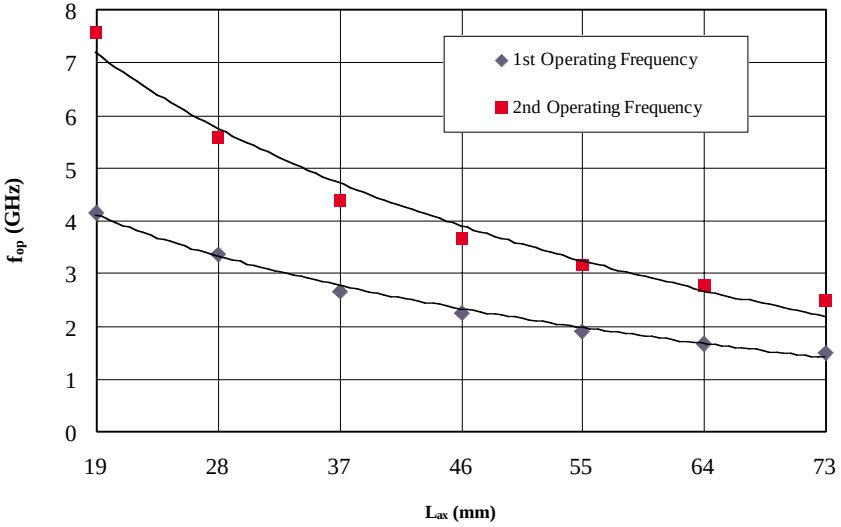

(c)

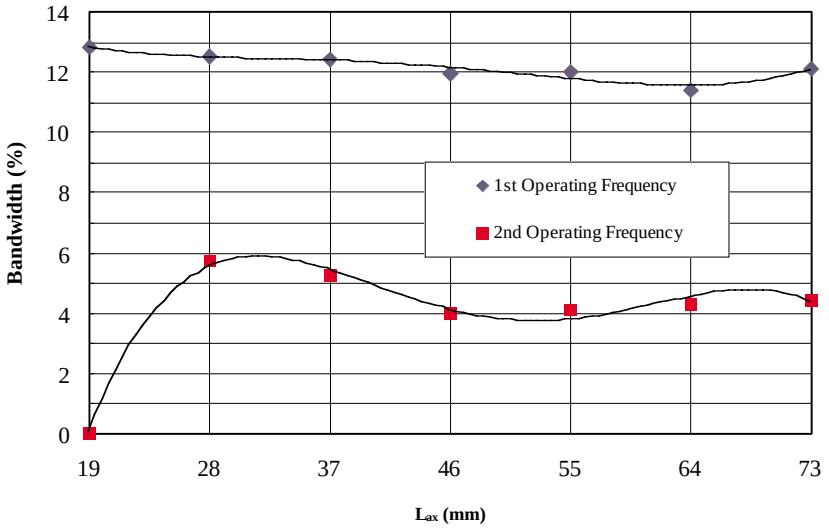

(d)

Figure 5. (c) operating frequencies (d) bandwidth of meander line antennas versus L_{ax} .

In addition to changing L_{ax}, different values of the substrate dielectric constant are adopted to examine their influence on both resonant frequency and impedance in the optimal case ($L_{ax} = 73\,\text{mm}$). From Figure 6(a), the operating frequency decrease with the increase of the dielectric constant. From Figure 6(b), when ε_r is less than 6, the change of ε_r can be used to tune the operating frequencies. When ε_r is larger than 6, the input impedance is becoming unacceptable for $50\,\Omega$ PCS application as clearly shown from the corresponding VSWR values in Figure 6(b). Figure 6(c) shows that the bandwidth values are also acceptable for values of $\varepsilon_r < 6$.

The effect of the dielectric slab thickness t_s is also investigated. It is found that the thickness of the dielectric slab changes the resonant frequencies within $0.1\,\text{GHz}$ for both the 1st and 2nd operating frequencies as shown in Figure 7(a). The 1st and 2nd operating frequencies are also in the vicinities of 3rd and 5th resonance, respectively. However, the changes of the input impedance are detectable as shown in Figure 7(b). When the thickness is small, the better VSWR is observed, but the bandwidth of the 1st band is reduced from 12 percent to 10 percent as shown in Figure 7(c). The empirical equations for the 1st and 2nd operating frequencies versus t_s are

$$f_{op1} = 1.5814 - 0.064\ln(t_s) \tag{3a}$$

$$f_{op2} = 2.5353 - 0.0577\ln(t_s) \tag{3b}$$

The empirical equations for the 3rd and 5th resonance impedance versus t_s are

$$\begin{aligned} R_{o3} = & -0.012729(t_s)^6 + 0.15862(t_s)^5 - 0.51952(t_s)^4 + \\ & 0.84411(t_s)^2 + 46.647 \end{aligned} \tag{4a}$$

$$\begin{aligned} R_{o5} = & \, 0.004196(t_s)^6 - 0.0051357(t_s)^5 + 0.16667(t_s)^4 - \\ & 0.47453(t_s)^2 + 46.998 \end{aligned} \tag{4b}$$

Finally, the effects of the width of the dielectric slab are also investigated for the antenna with $L_{ax} = 73\,\text{mm}$. From Figure 8, the variations of the operating frequencies and bandwidth due to the change of the slab width are insignificant. However, the effects on the input impedance are clearly noticeable from the VSWR values. The operating frequencies are in the vicinities of the 3rd and 5th resonance. When the width is less than $20\,\text{mm}$, this antenna performs as a good $50\,\Omega$

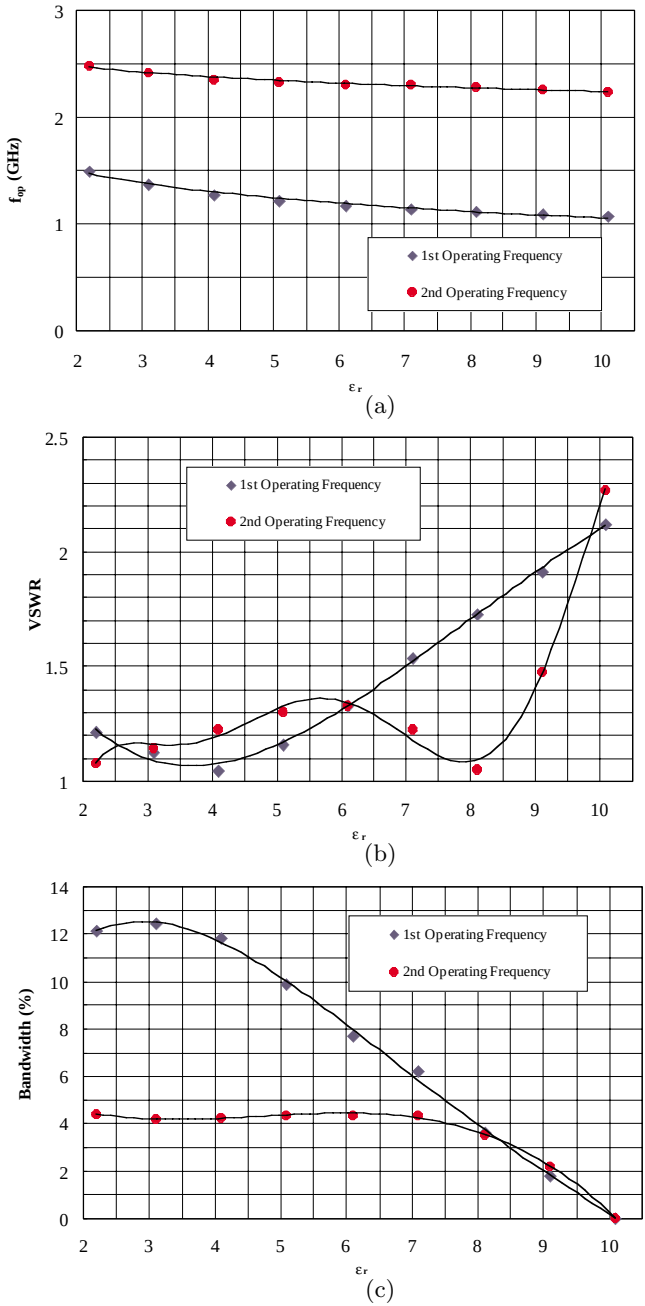

Figure 6. (a) Operating frequencies (b) VSWR (c) bandwidth of meander line antennas versus ε_r with $L_{ax} = 73\,\text{mm}$.

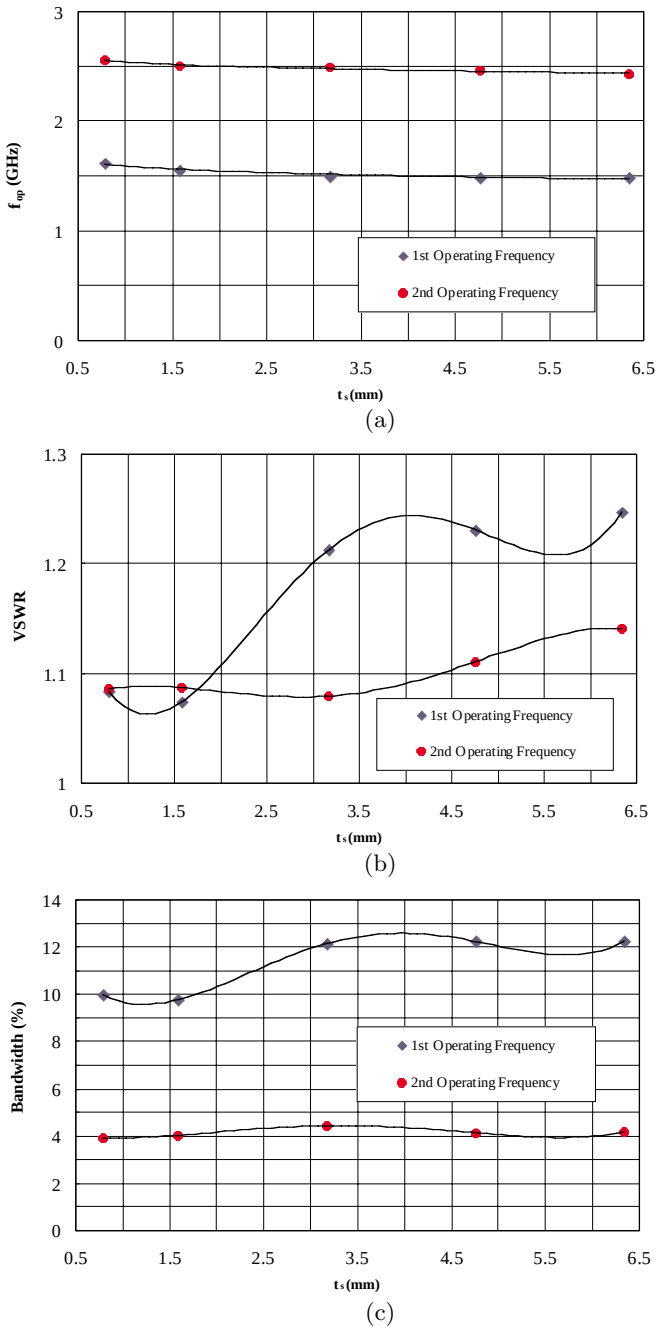

Figure 7. (a) Operating frequencies (b) VSWR (c) bandwidth of meander line antennas versus t_s with $L_{ax} = 73\,\text{mm}$.

dual band antenna. This feature can be applied to the antenna printed on a small circular cylinder whose curvature is comparably small to the wavelength to reduce the size of the substrate. The relation between the operating frequencies versus W_s can be described as

$$f_{op1} = 1.5262 - 0.0193 \ln(W_s) \tag{5a}$$
$$f_{op2} = 2.6080 - 0.0552 \ln(W_s) \tag{5b}$$

The relations between the 3rd and 5th resonance impedance versus W_s are

$$\begin{aligned} R_{o3} = {} & 1.4673 \times 10^{-7}(W_s)^6 - 1.6513 \times 10^{-5}(W_s)^5 + \\ & 5.8583 \times 10^{-4}(W_s)^4 - 0.0016801(W_s)^3 - \\ & 0.33882(W_s)^2 + 7.0505(W_s) \end{aligned} \tag{6a}$$
$$\begin{aligned} R_{o5} = {} & -1.0341 \times 10^{-6}(W_s)^6 - 1.4712 \times 10^{-4}(W_s)^5 - \\ & 8.2505 \times 10^{-3}(W_s)^4 + 0.23041(W_s)^3 - \\ & 3.3021(W_s)^2 + 21.699(W_s) \end{aligned} \tag{6b}$$

4. CONCLUSIONS

A detailed investigation for optimizing the printed meander line antenna with dual sleeves for personal wireless communication has been presented. Empirical equations are obtained and used to achieve a design in which an external matching network is not necessary. An additional fine tuning for the operating frequencies and input impedance is achieved by varying the dielectric slab parameters. The presented meander line with dual sleeves cover the frequency range 1.25 GHz to 3.0 GHz with VSWR less than 1.4 and bandwidth varied within 120–340 MHz, which may effectively support the upper PCS bands and the future 3rd generation cellular applications. The application around 0.8–1 GHz may be realized by extending L_{ax} and using a higher permittivity substrate to shorten the necessary increase of L_{ax}. Future studies will be focused on the optimization of the radiation pattern parameters.

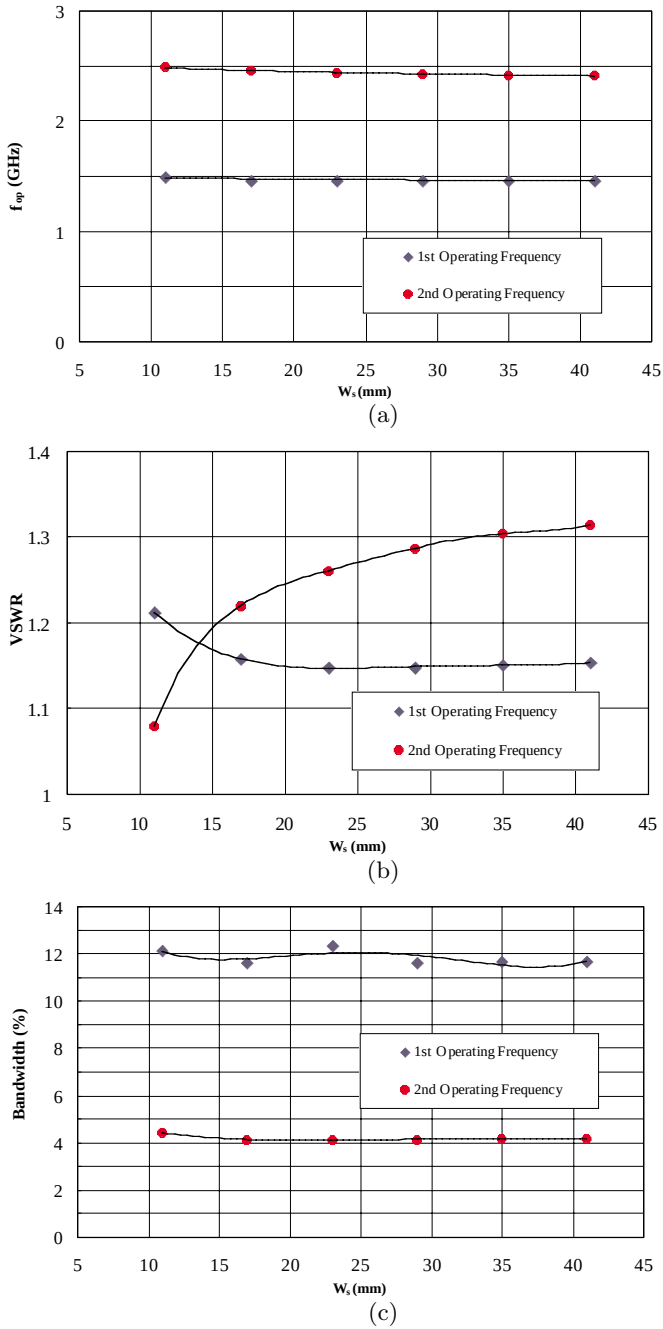

Figure 8. (a) Operating frequencies (b) VSWR (c) bandwidth of meander line antennas versus W_s with $L_{ax} = 73\,\text{mm}$.

REFERENCES

1. Nakano, H., H. Tagami, A. Yoshizawa, and J. Yamauchi, "Shortening ratio of modified dipole antennas," *IEEE Trans. Antennas Propagat.*, Vol. AP-32, No. 4, 385–386, April 1984.
2. Ali, M., S. S. Stuchly, and K. Caputa, "A wide-band dual meander-sleeve antenna," *Journal of Electromagnetic Waves and Applications*, Vol. 10, No. 9, 1223–1236, 1996.
3. Noguchi, K., M. Mizusawa, T. Yamaguchi, and Y. Okumura, "Numerical analysis of the radiation characteristics of the meander line antennas consisting of two strips," *IEEE AP-S Symposium*, 1598–1601, 1996.
4. Ali, M., S. S. Stuchly, and M. Okoniewski, "Characterization of planar printed meander line antennas using the finite difference time domain technique," *IEEE AP-S Symposium*, 1546–1549, 1997.
5. Elsherbeni, A. Z., J. Chen, and C. E. Smith, "FDTD analysis of meander line antennas for personal communication applications," *Progress in Electromagnetics Research Symposium (PIERS),* Cambridge, MA, July 1997.
6. Yee, K. S., "Numerical solution of initial boundary value problems involving Maxwells equations in isotropic media," *IEEE Trans. Antennas Propagat.*, Vol. 14, 202–307, 1966.
7. Berenger, J. P., "A perfectly matched layer for the absorption of electromagnetic waves," *J. Computat. Phys.*, Vol. 114, No. 2, 185–200, Oct. 1994.
8. Sheen, D. M., S. M. Ali, M. D. Abouzahra, and J. A. Kong, "Applications of the three-dimensional finite difference time domain method to the analysis of planar microstrip circuits," *IEEE Trans. Microwave Theory Tech.*, Vol. 38, No. 7, 849–856, July 1990.
9. Gedney, S. D., "An isotropic perfectly matched layer-absorbing medium for truncation of FDTD lattices," *IEEE Trans. Antennas Propagat.*, Vol. 44, No. 12, 1630–1639, Dec. 1996.